Experimental and Numerical Study of a Rotating Wheel Air Classifier

L. Karunakumari, C. Eswaraiah, S. Jayanti, and S. S. Narayanan
Dept. of Chemical Engineering, Indian Institute of Technology, Madras, Chennai 600 036, India

DOI 10.1002/aic.10349
Published online in Wiley InterScience (www.interscience.wiley.com).

Rotating wheel air classifiers are often used in many process industry applications. The internal geometry of these equipment is quite complicated and has not been investigated in detail. In the present study, the flow field inside a rotating wheel air classifier has been calculated using CFD techniques, taking full account of the internal geometrical features. The predicted overall flow rate and the flow pattern are in good agreement with measurements and flow visualization studies. The calculations show that the induced flow depends strongly on geometric parameters such as the location of the inlet and outlet ports and the type of shutters used. Trajectory calculations of single particles show that the particle motion is influenced principally by centrifugal force, air drag, and wall-rebound characteristics. The wall rebound is possibly one of the means of how large particles enter the fines stream, leading to low efficiency at high speeds or large particles. Experiments of the classification using angular and radial shutter vanes show distinct range of operability of each type. These results have been interpreted coherently in the light of the flow pattern and particle trajectory calculations. © 2005 American Institute of Chemical Engineers *AIChE J,* 51: 776–790, 2005
Keywords: size classification, air classifier, computational fluid dynamics, particle trajectories, grade efficiency

Introduction

Classification is the process whereby a collection of particles is separated into two or more fractions differing in some physical property. The separation is usually by size but may also be by other particle properties such as density and velocity. Size classification is an important unit operation in process industries and finds demanding applications in mineral processes, food processing, pharmaceutical, and toner or powder paint industries. The various types of size classifiers fall into two general categories (Lynch, 1977): those that separate by forces of fluid dynamics and those involving the possibility of passing through an aperture. The former is density-dependent, whereas particle density considerations do not enter in the latter scenario. Fluid dynamic size separation takes advantage of the differences in rates of travel of particles in a fluid arising from differences in particle size. If the rates of travel are also influenced by differences in densities, the separation is terminal sorting. Air classifiers belong to this category and can be grouped further into classes, depending on the direction of flow of the carrying current, which may be vertical, horizontal, or curvilinear. A variety of air classifiers have been described in Snow et al. (1984) and Wills (1992).

The generic mechanism of air classifiers is as follows. The feed material to be classified is suspended in an air stream and the coarse fraction is separated from the fine fraction and the air stream by aerodynamic drag, which usually overcomes another force, such as gravitational, inertial, or centrifugal force, or a combination of all three. Usually, the two important forces are the drag force and the centrifugal force. If the particle is small, the drag force will predominate and the particle will move with the air stream into the fine fraction. If the centrifugal force is greater than the drag force, particles will be deflected into the coarse fraction. The particle size for which centrifugal force

Correspondence concerning this article should be addressed to S. Jayanti at sjayanti@iitm.ac.in.

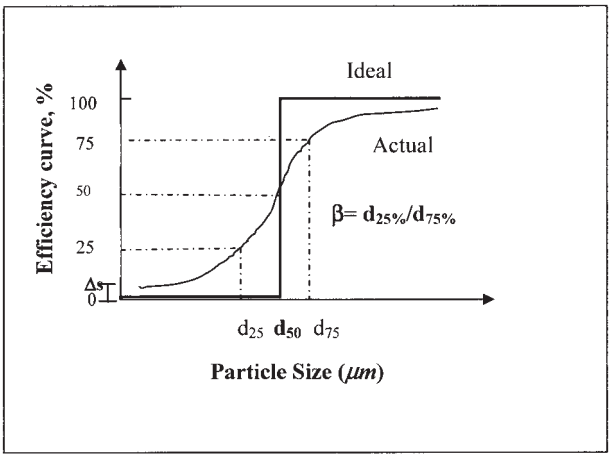

Figure 1. Ideal and actual efficiency curves in a size classifier.

equals drag force is called *cut size*. In principle, if the two forces are equal, the particle will be held in equilibrium. This equilibrium determines the cut point of an ideal classifier. The efficiency of air classifiers, such as air cyclones and rotating wheel air classifiers, is influenced by a number of additional parameters such as particle concentration, particle shape, and flow conditions including the inlet and outlet areas. The advantage of a rotating wheel air classifier is that it does not require any external compressor to send air as in an air cyclone. Also, the volumetric flow rate of air required for classification is much less in the rotating wheel classifiers, given that the centrifugal force needed for separation is realized by using an internal rotor. Optimized design and high centrifugal acceleration enable centrifugal counterflow air classifiers to work in the submicron range (Galk et al., 1999).

The performance of an air classifier can be measured (AIChE, 1993) in terms of three major parameters: (1) the cut size (d_{50}), (2) the size selectivity increment (ΔS), and (3) the sharpness of separation (β) related to a typical size selectivity curve (also known as grade efficiency curve), shown in Figure 1. Here, the size selectivity S_d (or grade efficiency) is defined as the ratio of the quantity of particles of size d in the coarse fraction to that in the feed. For proper classification, S_d should be low for small particles and high for large particles. With reference to Figure 1, the particle size that has a 50% probability of getting into the coarse fraction is called the cut size (d_{cut} or d_{50}). For an ideal classifier, the $S_d = 0$ for $d < d_{cut}$ and $S_d = 1$ for $d > d_{cut}$. No real classifier behaves ideally and some small particles enter the coarse fraction and some large particles are retained in the fine fraction. Thus, a typical S-shaped curve is obtained. The size selectivity coefficient (ΔS) characterizes the quantity of feed material that goes directly into the coarse fraction without classification and is given by the intercept on the abscissa of the extrapolated grade efficiency curve. The sharpness of separation (β) describes the effectiveness of a given classification. It is defined as d_{25}/d_{75}, that is, the ratio of particle size with a grade efficiency of 25% to the particle size at 75% grade efficiency. For a perfect classification it has a value of unity. The smaller the value of β, the poorer the sharpness of classification.

Although they are widely used, much of the information regarding rotating wheel air classifiers is patented and is not available in the open literature. In recent years, some systematic studies of rotating wheel classifiers have been reported in terms of generic influence of system and operating conditions on the above parameters. Clerc et al. (1999) carried out experiments using a Condux size classifier characterized by a rotor positioned vertically with feed material as fly ash (d_{80} of 94 μm) and studied the effect of rotation speed, air flow, and the feeding rate of fly ash. They found that the rotational speed of the rotor determined the cut size (which decreased with increasing speed), whereas the other parameters—the air flow rate, ash feeding rate, and the percentage of fine particles—primarily affected the quality of the extraction. They also studied the scaling effect by comparing the performance of a laboratory pilot with that of an industrial pilot and found that the two behaved in a similar way.

Galk et al. (1999) described the development of a rotating wheel classifier designed to work in the submicron range. The MikroCut MC classified particles from a few tens of microns down to submicron range. Using centrifugal acceleration of up to 15,000g, very fine particles were produced, such as talcum with 97% below 1.7 μm with a throughput of several 100 kg/h. To increase the efficiency of the classification, that is, to increase the yield, secondary air was fed into the classifier at the outer periphery of the hosing and entered the classification chambers to transport fine material through the rotor into the fine fraction. The secondary air improved the sharpness of cut, resulting in an increased yield from 73% up to about 94%. Because of high sharpness of the cut, the grade efficiency curves typically exhibited a fishhook-type of curve with some very fine particles appearing in the coarse fraction.

Although the importance of air flow within the classifier has been well recognized, detailed measurements have not been reported. Recently, Kolacz (2002) used on-line instrumentation from Malvern Insitec for particle size and concentration measurement to measure the particle size distributions at several locations in a forced-draft rotating wheel classifier developed at SINTEF (Trondheim, Norway). These show that significant variations exist within the classifier, which may have an important effect on the efficiency of classification and wear of the rotor blades. It was felt that a better understanding of the fluid flow within the classifier would promote a better understanding of the process. However, this has not been possible to date. Because a rotating wheel classifier has a complicated geometry with a combination of rotating fan blades and stationary guide vanes in passages of irregular shape, theoretical calculation of the flow field is not possible. The complicated internal details also render local measurements very difficult and this has not been attempted.

Against this background, numerical methods, in the form of computational fluid dynamics (CFD) simulations, are used in the present study to calculate the flow field. CFD, which deals with the numerical solution of the governing equations and constitutive laws of fluid flow, enables fairly accurate calculation of a single-phase flow field in equipment of arbitrary geometric complexity. In recent times, it has proved to be a useful analytical tool in the optimization of many devices commonly used in the process or chemical industries (Bakker et al., 2001). The application of CFD to cyclone and other types of gas–solid separators (Griffiths and Boysan, 1996; Wang et al., 2001) is well documented in the literature. Taking advan-

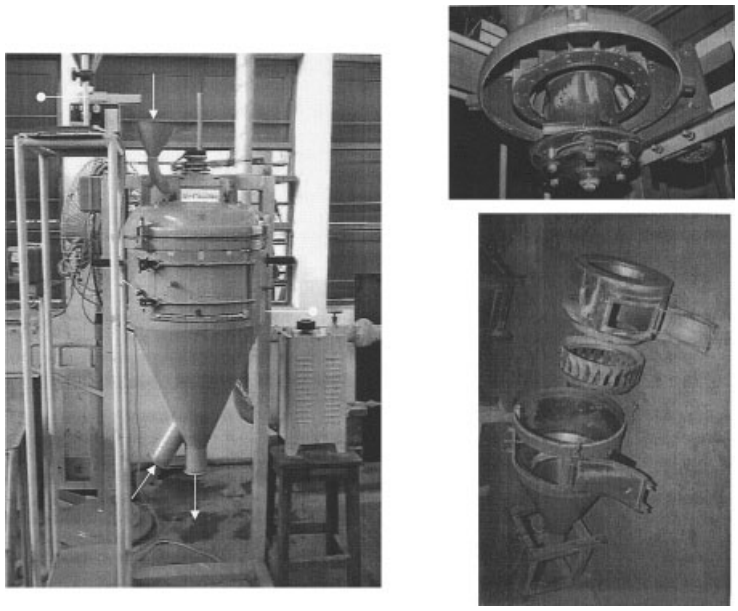

Figure 2. Rotating wheel air classifier used in the present study.

(a) Assembled view; (b) details of the internal structure.

tage of this, we report herein on the first detailed study of the flow field inside a rotating wheel air classifier. Several simulations have been carried out taking account of all significant details of the internal geometry, and influence of the principal design and operational parameters on the flow field has been brought out. These flow field calculations are then followed up by studies of typical particle-flow field interaction through Lagrangian simulation of particle trajectories. Flow visualization experiments and grade efficiency measurements were also carried out to complement the CFD studies. Together, these studies contribute to a better understanding of the operation of the rotating wheel classifier. Details of these studies and the results obtained are discussed below.

Details of the Calculation Methodlogy

Description of the equipment

The essential parts of the classifier used in the present study are: a cylindroconical vessel, a rotating wheel at the top with fan blades attached to it, rotating guide vanes (the position of which can be changed), a vibratory feeder, an internal hopper with a pipe extending through the outer shell, and shutters (angular or radial) connecting the inner and the outer compartments. These are shown as an assembled view in Figure 2a, whereas the internal details are shown in the exploded view in Figure 2b. These contain details of the rotating fan at the top, the inner cylindrical section, and the angular shutters (stationary guide vanes). Because of the rotation of wheel, air is sucked through the air inlet and goes up and comes into the annular region and comes out through the air outlet. Feed enters through the vibratory feeder and falls on the rotating wheel, where it is discharged in a radial direction by centrifugal force. All particles are of substantially the same density. Fine particles pass along with the entering air and are collected from the fine outlet. The coarse particles fall against entering gas stream and are collected from the air inlet pipe. In actual operations, the inlet and outlet ports are covered by gunny bags, which allow air to pass through but prevent the particulate matter from following suit. The air classifier used in the present study has an overall height of 0.95 m and a diameter of 0.51 m. The vibratory feeder has a capacity of up to 80 kg/h for rice husk and 180 kg/h for fly ash. A dimmerstat connected to the AC motor allows the speed of rotation to be changed continuously from 0 to 2400 rpm.

Geometrical modeling of the classifier for CFD calculations

As can be seen above, the internal structure of the classifier is fairly complicated; however, with the use of CFD codes (such as FLUENT and CFX), it is possible to calculate the single-phase flow field in an arbitrarily complicated geometry in a reasonably accurate manner by numerically solving the Navier–Stokes equations governing the fluid flow with models of turbulence (Ferziger and Peric, 1999). A complete solution to the classification problem, however, is beyond the scope of CFD, given that a number of physical phenomena such as particle–wall interactions, particle–particle interactions, particle–turbulence interactions, and turbulence in two-phase systems, cannot be taken into account in a reasonably rigorous manner. Thus the likely interaction between typical particles that need to be classified and the predicted flow pattern within the classifier is studied by simulating the trajectories of particles of different sizes. In the present study, a commercially available CFD code, FLUENT 5 (developed by Fluent USA, Lebanon, NH) has been used for CFD simulations. FLUENT 5 is an unstructured general-purpose solver for complex flows ranging from incompressible (low subsonic) to mildly compressible (transonic) to highly compressible (supersonic and hypersonic) flows. It has a preprocessor, GAMBIT, which can be used to define the flow domain and its discretization into

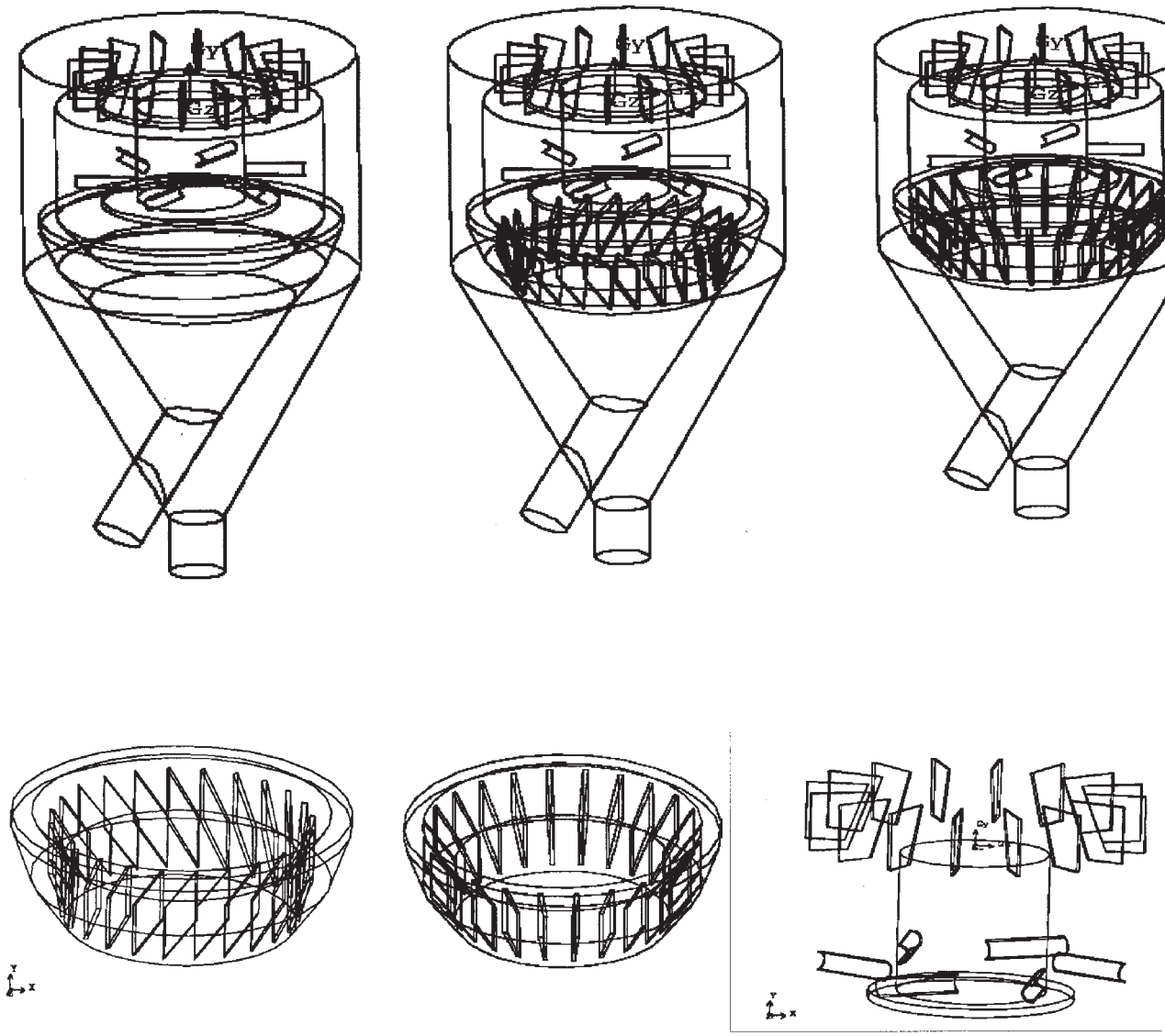

Figure 3. Wire-frame models.

(a) The three configurations used in the present study, and details of (b) angular-vane shutters, (c) radial-vane shutters, and (d) rotating parts.

small grids and to incorporate the appropriate boundary conditions.

A three-dimensional model was created in GAMBIT using an unstructured grid. Preliminary experiments showed that the type of the stationary guide vanes or shutters—angular (Figure 3a) or radial (Figure 3c)—had an important effect on the classification. To bring out this effect more clearly, three configurations (Figure 3a) were studied in the present case: no shutters (open configuration) angular shutters and radial shutters. Experiments, however, could not be conducted with the last configuration. A total number of cells ranging from 400,000 to 600,000 for different configurations was used to construct an unstructured mesh with tetrahedral cells for the flow domain within each classifier configuration. The geometry was created to the actual dimensions and thus no scaling was involved. The quality of grids, in terms of skew and aspect ratio, was checked. All the geometric details of the equipment, such as the rotating blades of fan, rotating guide vanes, slanting air inlet, and stationary vanes at the top of the conical section were incorporated into the calculation, as can be seen in the "wire-frame" model of the three configurations (Figure 3a). The guide vanes in the angular configuration were at an angle of 35° from the tangent (Figure 3b), whereas they are perpendicular in the radial vane configuration (Figure 3c), the number of vanes in each case being 24. Finally, the details of the rotating set of vanes, consisting of 16 fan blades and seven guide vanes near the bottom of the rotating part, are shown in Figure 3d; these are common to all the configurations. Except for the chamfering of the corners (which becomes a subgrid phenomenon in the present calculations and taking account of chamfering would have required a prohibitively huge grid), these details match with those of the experimental conditions in terms of size, shape, and number.

Because the number of cells was already too high and because the convergence of the iterative solution slow, no formal grid-independence study has been conducted. However,

calculations have been repeated for two cases by increasing the number of cells from 400,000 to 576,000 using the grid-adaptation procedure in FLUENT, where the grid was refined locally based on the local axial velocity gradient. The overall flow pattern remained the same. The axial velocity profiles near the center of the cylindrical section predicted by the coarser and the finer grids were compared and were found to be nearly identical. Although this would, in itself, not constitute a rigorous grid-independence test (for which an order of magnitude increase in grid density may be necessary), this exercise shows that the grid is sufficiently fine throughout the domain (all air passages having been accurately resolved) to capture the details of the flow fairly well.

Equations solved

Briefly, the equations solved to obtain the flow field consist of the equations of conservation of mass and momentum; the equations of the standard k–ε model (Launder and Spalding, 1974) to take account of turbulence effects; a moving reference frame model (Murthy et al., 1994) to take account of the motion of the rotating blades; and a set of drag, lift, and other correlations constituting the discrete phase model used for particle trajectory calculations. Apart from the assumptions involved in the above models, the only other assumptions involved in the calculation are that the flow of air is Newtonian and that its properties are constant. Thus there is no empiricism in dealing with the blade motion. The rotating reference model allows the calculations to be done on a steady-state basis and has previously been used, for example, by the present authors to calculate flow in a helical impeller-driven mixing system (Shekhar and Jayanti, 2003). Standard wall functions (Wilcox, 1993) with zero-slip condition were used at the walls, whereas the inlet and the outlet were treated as constant-pressure planes with *z*ero pressure relative to the atmospheric pressure. The standard k–ε model used did not incorporate any corrections for swirling flow or for streamline curvature because it is not known to what extent these are applicable to the current flow situation. To assess the relative sensitivity of the predictions to the turbulence model, additional calculations have been attempted with the swirl-dominated flow version of the RNG k–ε model and with the Reynolds stress model, both of which are available as standard options in the FLUENT code. It is thought that the former, which incorporates correction factors to account for the effect of swirl on the turbulence, would be more suitable for the present case. The Reynolds stress model is a higher level turbulence model than the k–ε family of models and would be capable of taking account, inherently (that is, without *ad hoc* modeling), the effects associated with streamline curvature. Although these models have proven to be superior for some specific cases involving swirl, their applicability to problems of current geometrical complexity has not been tested. Indeed, it is found that the more sophisticated Reynolds stress model did not converge at all for the cases investigated in the present study. The RNG k–ε model was found to be less robust than the standard k–ε model and for the four cases tested, the predicted flow field differed only slightly from that predicted by the standard k–ε model. Although this cannot be said to be the last word on it, in the absence of detailed flow-field measurements in the classifier, the results obtained with the standard k–ε model can be treated as being fairly representative.

The particle–flow field interaction is studied using a particle-trajectory analysis. Here, the trajectory of a discrete phase particle is calculated by integrating the momentum balance on the particle in a Lagrangian reference frame, which can be written (for the x-direction in Cartesian coordinates), as

$$\frac{d(u_p)}{dt} = F_D(u - u_p) + g_x(\rho_p - \rho)/\rho_p$$

where $F_D(u - u_p)$ is the drag force per unit particle mass; u and u_p are the fluid and particle velocity components in the x-direction, respectively; and ρ and ρ_p are their corresponding densities. The drag coefficient C_D is obtained from the empirical correlation of Haider and Levenspiel (1989). The effect of other forces such as the Bassett force and the virtual mass is neglected. A stochastic modeling approach, in which the particle interacts with a series of randomly oriented, randomly sized turbulent eddies of random distribution of lifetimes, is used to represent the turbulent dispersion of particles. All the side walls and vanes are treated as being reflective, with a restitution coefficient of 0.8 for both normal and tangent components. The inlet and the outlet surfaces are treated as "escape" surfaces through which the particle leaves the flow domain and ceases to be of further interest.

Numerical details

All the governing equations for the fluid flow calculation are discretized using the finite-volume method (Ferziger and Peric, 1999). This method involves formal integration of the governing equations of the fluid flow over all the (finite) control volumes of the solution domain and the substitution of a variety of finite-difference type approximations for the terms in the integrated flow equations representing the process such as diffusion and sources. This procedure converts the integral equations into a system of algebraic equations. The discretization adopted in the present study is formally second-order accurate, including for the convective terms for which a second-order accurate upwinding scheme is used. The SIMPLE (Semi-Implicit Method for Pressure-Linked Equations) formulation involving a pressure-correction equation (Patankar, 1980) is used to evaluate pressure from the continuity equation. An overall sequential and iterative solution of the set of discretized and linearized algebraic equations is carried out to eventually obtain the flow field. The iterative solution was carried out until the residual factors, which indicate by how much the governing equations are not satisfied at the discrete level, are below 0.0001 for each equation. Once the fluid flow field is obtained, the trajectory equations are solved by stepwise integration over discrete time steps. Because the particle trajectory calculations were taking an inordinate amount of time, the two-way coupling between the two phases could not be included; thus, the effect of the particulate phase on the air flow was not considered. The results therefore would be applicable only to "low" loading of the particles. As shown below, the calculations do, however, bring out important features of the classification process.

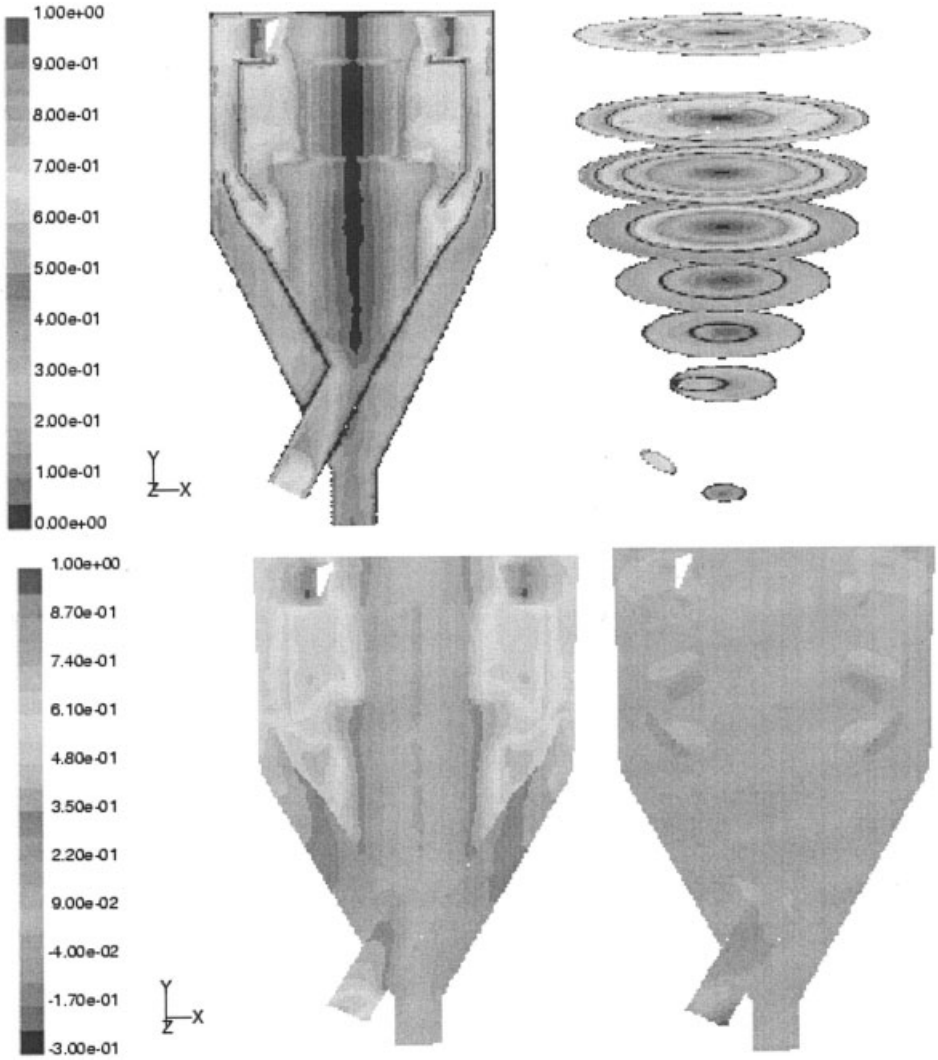

Figure 4. Contours of (a) velocity magnitude in vertical and horizontal sections, and contours of (b) tangential velocity component and (c) radial velocity component in the vertical plane for the "open" configuration without vanes at 1450 rpm.

Results

Typical results

Velocity Contours. The variation of the velocity within the classifier for the first configuration, that is, without stationary guide vanes, for a fan speed of 1450 rpm is shown in Figure 4a in the form of contours of the magnitude of velocity in the vertical plane and at various horizontal sections. Here, the velocities are nondimensionalized by dividing them by the tip velocity of the fan blade. The dimensionless tangential and radial velocity components are shown in Figures 4b and c, respectively, in a vertical plane. It can be seen that the flow induced is primarily tangential of almost solid body–like rotation with increasing tangential velocity as the distance from the axis increases. However, significant axial and radial components are also present. The axial velocity component (positive value indicating upward velocity) is of particular interest because it can potentially entrain small particles and is shown separately in Figure 5a in a vertical plane. From this figure it can be clearly observed that, in the upper cylindrical part of the classifier, there are positive velocities in the inner cylindrical region and negative velocities in the annulus region. This implies that air is moving up in the inner cylinder and is coming down again in the annulus region. This means that there is a downward axial flow in the annulus. Large radial velocities (30 to 40% of the tip speed) are found near the fan blade and the stationary guide vane location. The axial flows in the inner cylindrical section and in the outer cylindrical annulus are also high and are of the order of 30 to 40% of the tip speed.

The combination of the axial and radial velocities in the upper portion of the classifier is such that an overall secondary circulation is created in the vertical plane. This is clearly seen in the axial velocity profile at nearly midheight of the cylindrical section shown in Figure 5b. Also indicated here is the extent of the inner cylindrical region and the outer annulus region. It can be seen clearly that large negative velocities are created in the outer annulus, whereas the axial velocity component is positive in the inner cylindrical region. An integration of the secondary flow over the area of the outer annulus

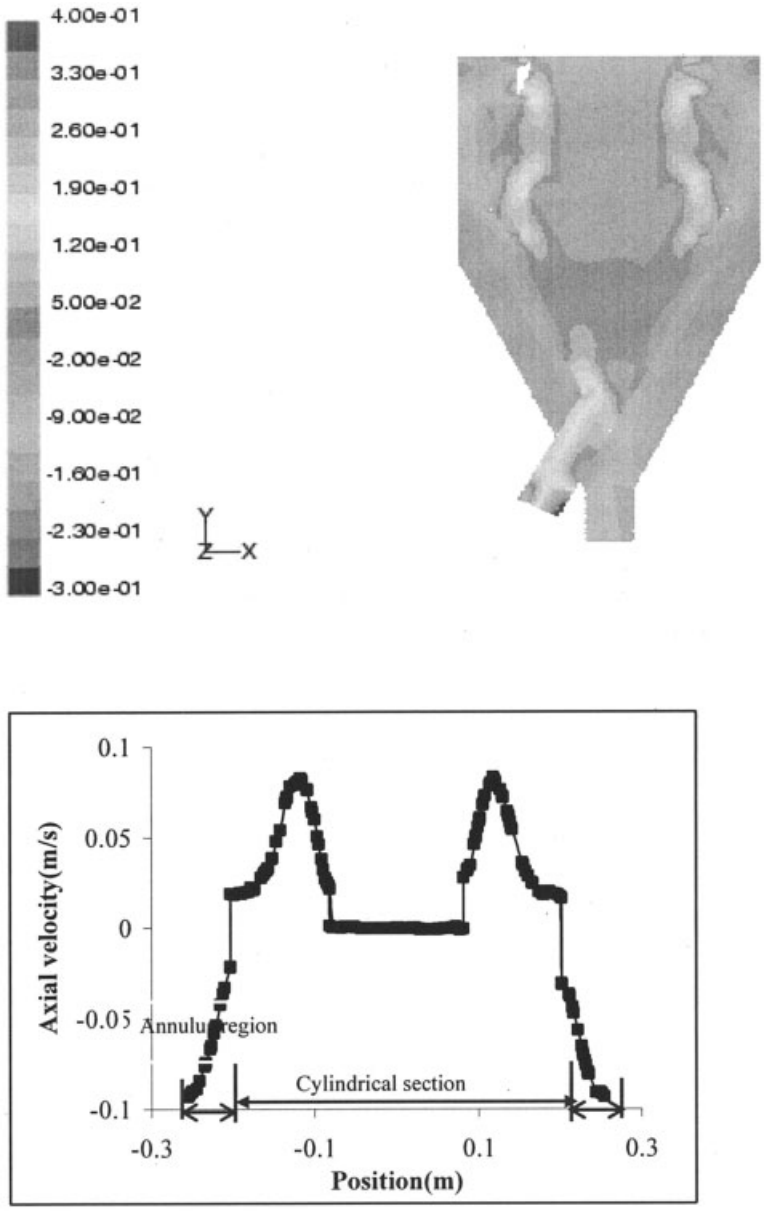

Figure 5. (a) Axial velocity contours at 1450 rpm for the open configuration without vanes, and (b) axial velocity profile at about midheight (0.1 m from the top) of the cylindrical section.

indicates that this secondary flow is higher than the net flow rate by a factor 8 for this configuration. The region near the axis of rotation, however, is nearly stagnant and a very low velocity fluid is present there. Generally speaking, higher velocities are created inside the classifier for this configuration than that with the radial or angular vane configuration.

Pressure Contours. The total pressure contour for the first configuration without vanes at 1450 rpm along vertical section is shown in Figure 6. Here, the total pressure is nondimensionalized by dividing it by the kinetic head based on the tip velocity, that is, $(1/2)\rho u_t^2$. The predominantly tangential motion of the fluid leads to a vortex type of formation with very low pressure around the axis. The kinetic energy imparted by the rotating fan blades is converted into pressure head in the annulus region leading to a large pressure there. This high pressure in the annulus leads eventually to the flow going out through the bottom outlet. It is interesting to note that the pressure in the inlet section of the pipe is more than that along the axis. This induces the flow into the classifier through the air inlet.

Axisymmetry of the flow

The above results are shown in the vertical plane passing through the inlet pipe. Comparison of these predicted velocity and pressure contours with those in a vertical plane perpendicular to it showed that the flow field was nearly the same except for the region near the inlet pipe. Thus the flow is nearly axisymmetric and it would be sufficient to examine it in one vertical plane. However, the flow cannot be mod-

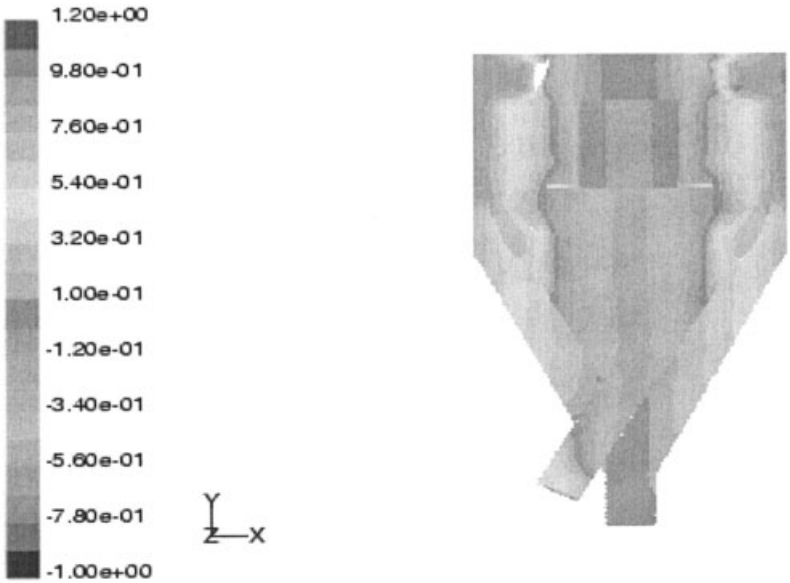

Figure 6. Total pressure contours for the open configuration without vanes at 1450 rpm in the vertical plane.

eled as a two-dimensional axisymmetric flow. It was found that replacing the slanting inlet with a coaxial inlet within the outlet pipe (which makes the geometry axisymmetric) led to a huge overprediction (by a factor of 8) of the net induced air flow rate. A full three-dimensional (3-D) calculation incorporating all the geometric details accurately is therefore necessary for correct results.

Effect of rotational speed of fan

A number of calculations have been done for the three configurations over the range of rotational speed between 900 and 2400 rpm. It was found that the dimensionless pressure and velocity fields nearly were alike for 900, 1450, and 2400 rpm, except for some minor changes near the axis and near the fan blades. This indicates that the velocity field scales linearly with fan speed and pressure with the kinetic head based on the tip speed. Indeed, the predicted dimensionless axial velocity profiles at 900, 1450, and 2400 rpm collapse onto a single curve. Similar results were obtained for the other stationary vane configurations.

Effect of type of stationary vanes

Three stationary vane configurations—the open, the angular, and the radial configurations—have been investigated in the present study. All three configurations show predominantly circumferential motion in the upper half (cylindrical part) of the classifier. The radial vane configuration has a relatively low tangential velocity in the inner cylindrical part compared to the angular vane configuration. An integration of the secondary flow over the area of the outer annulus indicates that this secondary flow is higher than the net flow rate by a factor 2 for second and third configurations, that is, with angular vanes and radial vanes. As noted above, the secondary flow is much stronger, by a factor of 8, for the open configuration.

Another distinguishing feature of these flows is the secondary flow pattern. Examination of these flow fields reveals that a sustained secondary flow is created in the vertical plane. The strength and direction of this flow depends on the stationary vane configuration. When there are no vanes, a strong downward flow in the annulus region of the classifier is observed. This is present to a lesser extent with the angular vanes, although there is an upward axial flow in the annulus with the radial vanes. This is illustrated in Figure 7, where the predicted nondimensional axial velocity profile at nearly midheight of the cylindrical portion is drawn for the two configurations. The axial velocities are negative (downward) in the inner cylindrical section and positive in the outer annulus section for the radial vanes.

An examination of the predicted nondimensionalized pressure field for the three configurations showed that the pressure variation within the classifier is the largest with the radial vanes, whereas the open configuration gives rise to the smallest pressure drop. This is consistent with what is expected because the introduction of vanes disturbs the tangential flow pattern. This disturbance increases with increasing blade angle. This leads to the highest pressure losses in the classifier for the radial configuration where the shutter vanes are perpendicular to the dominant tangential velocity component.

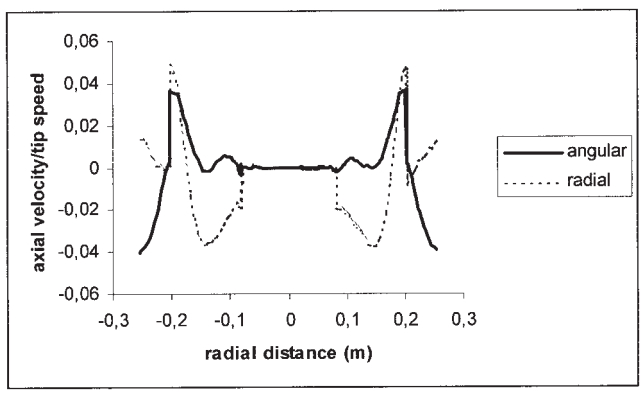

Figure 7. Axial velocity profile at about midheight of cylindrical section for angular vanes at 1450 rpm.

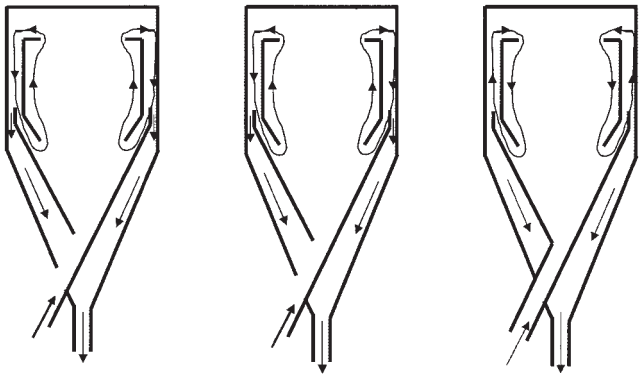

Figure 8. Flow pattern in the vertical plane for the three configurations.

The overall flow pattern set up in the three cases is schematically shown in Figure 8. It is seen that a considerable difference exists in the pattern near the junction of the cylindroconical section. As will be shown later, this difference in the flow pattern leads to significantly different classification behavior in the two vane configurations.

Validation of CFD results

Although CFD simulations are based on the numerical solution of fundamental equations of mass and momentum, a number of approximations are introduced in solving these and additional constitutive equations (such as those related to turbulence modeling). In view of this, experiments have been conducted to validate the CFD predictions. These include the measurement of the volumetric flow rate of air induced by the rotation of the fan and flow visualization studies.

Flow Rate Measurements. Measurement of air flow rates at different rotational speeds was carried out using two techniques: a turbine flow meter and a traversing pitot tube connected to a micromanometer. Measurements were carried out at the air outlet section. In the case of the turbine flow meter, the outlet was connected directly to the flow meter and the cumulative volumetric flow rate was directly read from the meter. In the case of the pitot tube, the measurements were carried out at several points by traversing the pitot tube along the diameter horizontally in two mutually orthogonal directions. The resulting velocity profiles were integrated to give the overall volumetric flow rate. Each profile measurement was carried out three times to verify repeatability. These were found to be matching closely and an average value was taken to calculate the flow rate.

Velocity profiles obtained from the pitot tube were found to be nearly axisymmetric and a typical turbulent-like velocity profile was obtained. The flow rate measurements were carried out over a range of fan speeds and the results obtained are compared in Figure 9 with the predictions of the CFD simulations. There is good agreement between the results obtained with the two experimental techniques as well as between experiments and the CFD results. As expected from the linear scaling of the velocity field the fan speed described above, a nearly linear variation of the volumetric flow rate with rpm is found in the experiments.

Flow Visualization Studies. Some flow visualization studies of the flow pattern inside the classifier were conducted to verify the CFD-predicted dependency of the flow pattern on the bottom stationary vanes, which can be either angular or radial. These were done by examining the deflection of small strings placed at a large number of locations on the inside wall of the conical bottom, cylinder, and the outer annulus. Observations were made by replacing the metal door by a transparent polythene sheet. Along with lighting from the bottom, this afforded a restricted view into the classifier under operating conditions. Because the use of actual particles of fly ash made the air foggy and practically opaque, visualization was restricted to air flow alone. Additional studies were conducted by releasing small foam cubes into the flow path from the top and also through the air inlet. These studies showed that the main motion in the classifier was indeed circumferential, especially in the cylindrical part of the classifier, both inside the cylinder and in the outer annulus. As predicted by CFD, with both radial and angular vane configurations, a secondary flow existed in addition to the main circumferential motion. In the case of the angular vanes, the secondary, recirculatory motion was present in the vertical plane with flow going up from the inside part into the outer annulus through the fan blades located at the top and returning through the stationary vanes located at the end of the cylindrical portion. In the case of the radial vanes, the secondary recirculatory motion was in the reverse direction, that is, flow going up from the inside part to the annulus region through the bottom stationary radial vanes and then coming into the cylindrical section through the top rotating blades. Even though no measurement of this flow pattern was possible, deflection of the strings indicated the flow rate here to be much higher than the net flow going through the outlet. The direction of this flow in the annulus was downward for angular stationary vanes and upward for radial stationary vanes. The overall flow pattern obtained from CFD simulations (Figure 8) is consistent with these visual observations.

Particle Trajectory Calculations

Typical particle trajectories

A typical result obtained from the particle trajectory calculations for a 1-micron particle going through the flow field, set up by the fan blades rotating at 1450 rpm with an open

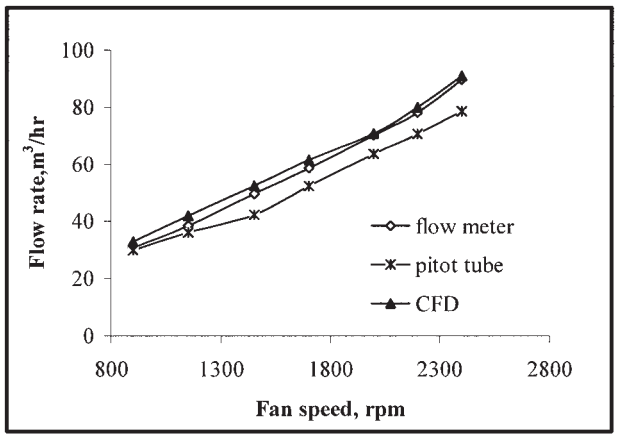

Figure 9. Comparison of calculated and measured air flow rates at the air outlet with angular vanes.

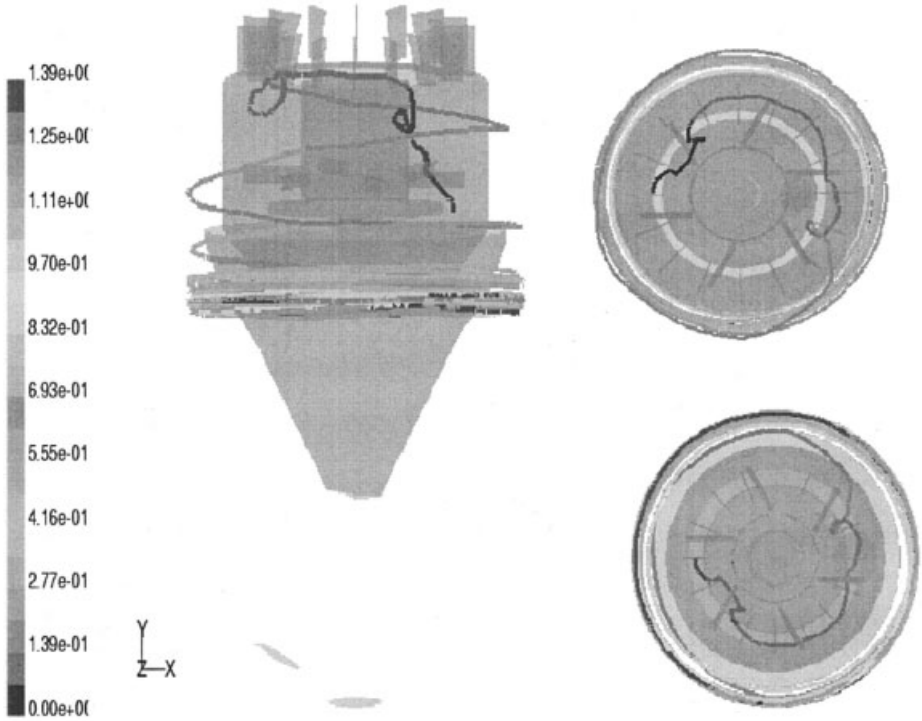

Figure 10. Typical particle trajectory for a 1-micron particle injected at the tip of the feed plate at 1450 rpm for the open configuration without vanes in three different views.

configuration, is shown in Figure 10 in three different views: as seen from the front, from the top, and from the bottom. To identify the relative position of the particle, the inlet, the outlet, all the rotating parts including the fan, feed plate, and guide vanes, and the inner cylindroconical wall are shown. Details of these can be seen in one or more of the three views. The solid walls of these parts have been made semitransparent so as to render the particle track more visible. The particle trajectory itself is colored by the residence time of the particle in the classifier and a scale indicating the color code is attached to the figure.

The particle shown in Figure 10 has a density of 1900 kg/m^3 (corresponding to that of fly ash) and is released from the edge of the feed plate. It can be seen that the particle, being small, is severely affected by the turbulence in the air phase and follows a jagged path. However, the mean motion corresponds to that of the air flow. It is soon caught up in the recirculation loop in the upper cylindrical portion and is gradually lifted up while still following a predominantly circumferential motion. It then exits the inner cylindrical portion through the top and slowly drifts down the annulus and finally into the conical annulus to be delivered into the fine fraction. The top view shows clearly the circumferential motion near the top of the cylindrical section, whereas the bottom view shows the decreasing radius of the circumferential path as the particle descends into the conical annulus.

The path taken by a particle through the classifier is influenced by a number of parameters such as the size, density, location of the particle as well as the speed of rotation, type of vanes, and so forth. The influence of these parameters is studied below.

Parametric influence on particle motion

One of the primary factors influencing the path of fine particles is the vane configuration. The trajectory of a 1-micron particle released from the same position with the angular vane configuration is shown in Figure 11a. The path is similar to that for the open configuration except for the fact that the particle goes through more revolutions before reaching the top. This can be attributed to the fact that the strength of the secondary recirculation is much higher with the open configuration than with the angular vane configuration. The descent in the annulus part is also slower for the angular vane configuration, which confirms this trend.

The paths obtained for the radial vane configuration for two cases with identical particle characteristics and initial position are shown in Figure 11b. It is seen that, unlike in the earlier cases, the particle descends into the central cylindrical region, which is consistent with the expected recirculation pattern in the radial vane configuration. The particle then rises through the gap and follows two different paths: it is entrained by the secondary recirculation and rises in Figure 11b (i) while it is entrained by the downward flow into the outlet and descends into the conical section in Figure 11b (ii). This is consistent with the flow split at this location, as shown schematically in Figure 8.

The trajectories of particles of different sizes can be very different. This is illustrated in Figure 12 where the trajectories of particles of 10, 25, 50, 100, 200, 300, and 400 μm are shown for a fan speed of 1450 rpm with the angular vane configuration. These particles are released near the inside conical wall about 1/3rd height from the bottom of the cone. These figures

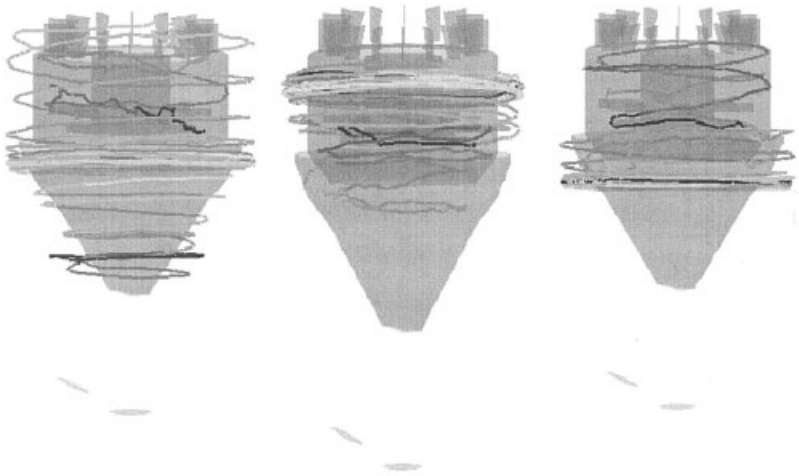

Figure 11. Typical particle trajectory for one micron particle injected at the tip of the feed plate at 1450 rpm for (a) the angular vane configuration and (b) for the radial vane configuration with the particle going (i) up and (ii) down in the annular passage.

reveal some interesting patterns. It is seen that the 10-μm particles follow the flow and are carried upward by the secondary recirculation. Particles of intermediate sizes, in the 25 to 100 micron range, are carried up with increasing speed to the top of the conical section. However, these escape into the outer annulus part and show a tendency to come down while still following a nearly circumferential path. Large particles, of 300 and 400 microns, follow an increasingly shorter path toward the top of the conical section and then continue to go up in the outer annulus, contrary to the downward flow of the secondary motion in this region.

Closer examination of these tracks revealed that this strange

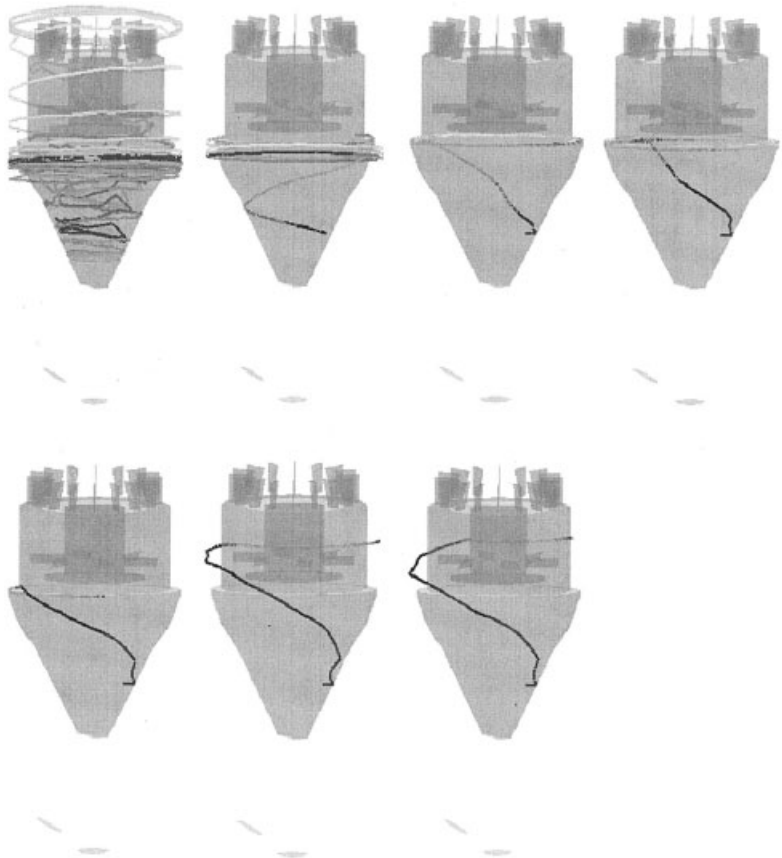

Figure 12. Trajectories of particles injected near the wall of the conical section in the angular vane configuration at 1450 rpm for particle sizes of 10, 25, 50, 100, 200, 300, and 400 μm.

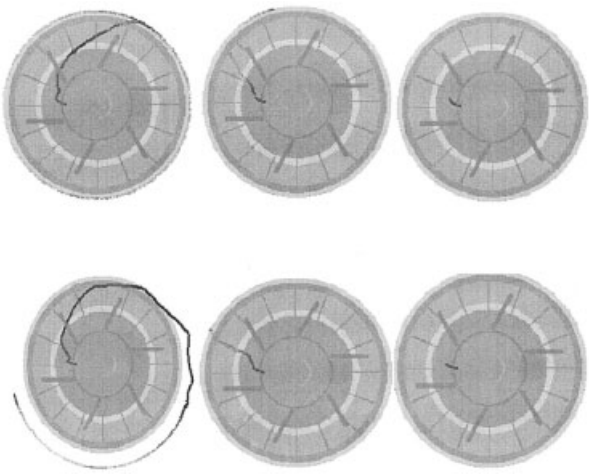

Figure 13. Top views of particle trajectories of size (a) 100 μm and (b) 300 μm for coefficients of restitution 0.8, 0.5, and 0.2.

behavior arises from a combination of centrifugal force, particle inertia, the drag of the secondary flow, and interaction with the wall. Small particles have relatively less inertia and are more easily diverted by the air drag. Thus, they tend to follow a more circumferential motion as can be seen in the tracks for the small particles. As the particle size increases, the particles suffer higher centrifugal forces and they increasingly detach themselves from the circumferential motion of the air. Also, they are more highly accelerated toward the wall and collide with a higher velocity. Because the normal restitution coefficient is specified as 0.8, and because the wall of the cone is at an angle, the particles attain a significant upward velocity upon rebounding from the wall. The larger the particles, the higher the upward velocity and the faster they reach the top of the conical section. This can be seen clearly in the tracks and the residence times for the large-size particles. When they reach the top of the conical section, the large particles still retain a significant amount of upward velocity. This, coupled with increased radial acceleration and further rebounding, takes them through the gap into the outer annulus where they continue their upward motion resulting from their large inertia. This repeated movement toward the wall and then rebounding away from it can be clearly seen in the tracks for the large-size particles in Figure 12.

Thus, the motion of particles in the classifier in the typical range of interest (50 to 500 microns) is influenced strongly by the centrifugal force and the wall–particle interaction and to some extent by the secondary recirculation that is set up. The importance of wall rebound is illustrated in Figure 13, where the tracks of 100- (Figure 13a) and 300-micron (Figure 13b) particles are shown with restitution coefficients of 0.8, 0.5, and 0.2. It can be seen that, with decreasing restitution coefficients, the particles lose their tendency to climb the conical wall. Because these are too large to be carried away by the upward gas flow, they remain close to the bottom of the cone and will eventually be collected in the coarse fraction.

The effect of gravity is rather small in this scenario. Comparison of the tracks for 1, 25, 100, and 300 particles under normal gravity conditions, and with gravity increased by a factor of 10, 100, and 1000 shows that the effect of gravity is negligible for small-size particles and their motion is strongly influenced only by the air drag. For very large size particles, the effect of inertia is such that a 1000-fold increase in gravity is required to make them come down. Even in the intermediate range, a 100-fold increase in gravity appears to be required to make the effect of gravity felt. Thus, on the whole, it can be said that the effect of gravity, under normal gravity conditions, is nearly negligible across the range of particle sizes.

Size Classification Experiments

Experimental procedures

The experiments were conducted using fly ash and rice husk. The fly ash was obtained from the Ennore Thermal Power Station, Chennai, India. It had a feed size (d_{80}) of 190 μm and was found to be in the operating range of the classifier. Thus, apart from drying, no further treatment was given to it. The raw rice husk was obtained from the market in one lot and was put through a pin mill to reduce the size (d_{80}) to 550 μm. Specific gravities of the fly ash and the rice husk were determined using a standard specific-gravity bottle and were found to be 1.9 and 0.60, respectively. The experiments were conducted and analyzed in accordance with the AIChE (1993) recommendations. A vibratory sieve shaker was used to determine the size distribution of the feed and both the coarse and the fine fractions. The measurements were conducted thrice to verify the repeatability of the results. The effect of three process parameters—the impeller speed, the feed rate of particles, and the type of shutter vanes—was studied and the results are interpreted here in the light of the results from the CFD calculations described above.

Parametric influence on classification

Effect of Rotational Speed. The effect of rotational speed of wheel and the feed rate on the cut size (d_{50}) is summarized in Figure 14a. Here, the typical variation of the cut size with speed is shown for three feed rates: 10, 20, and 40 kg/h of rice husk with the angular vane configuration. Similar results have been obtained for other conditions, that is, with radial configuration and with fly ash as the feed material instead of rice husk. It can be seen that, typically, the cut size increases as the fan speed increases for a constant feed flow rate. This can be attributed to the stronger secondary flow that is created at higher fan speeds within the classifier. Because the flow field scales linearly with the fan tip speed, the higher the rotational speed, the stronger will be the secondary circulation and the higher will be axial velocity. It has also been shown above that the particle motion of intermediate sizes is strongly influenced by the air flow. Thus, a stronger recirculation enables even larger particles to be carried away into the annulus (and ultimately into the fine fraction). This shifts the grade efficiency curve to the right as the fan speed is increased, resulting in an increase in the cut size.

Typical grade efficiency curves obtained at speeds of 1200, 1450, and 1950 rpm at a constant feed rate of 80 kg/h of rice husk are shown in Figure 14b. These indicate that the efficiency of collection in the coarse fraction decreases for a given size as the speed of rotation increases. It is also interesting to note that the collection efficiency decreases monotonically for

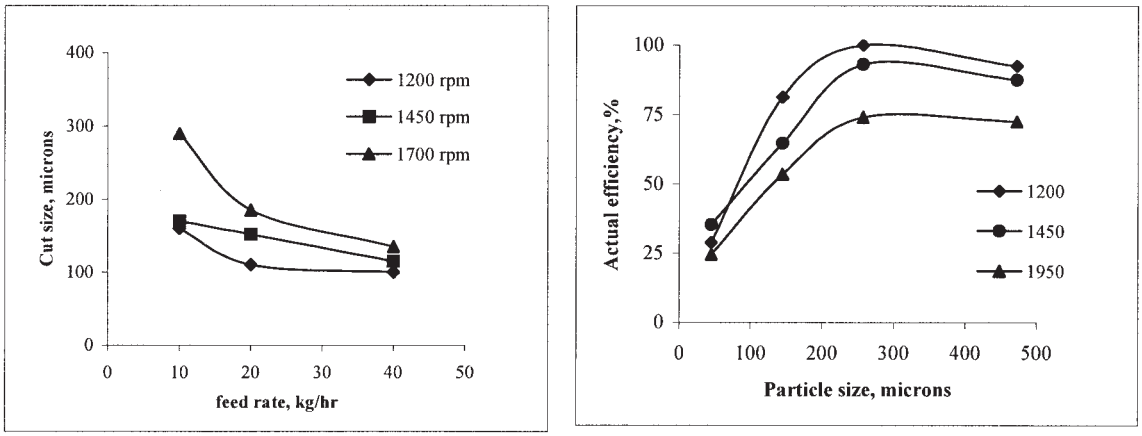

Figure 14. (a) Effect of feed rate and wheel speed on cut size; (b) actually efficiency curves at different speeds at a feed rate of 80 kg/h for rice husk for the angular vane configuration.

all large particle sizes. The reason for this can be twofold: (1) the increased drag of the stronger recirculation and (2) the increased centrifugal force that would enable large size particles to go into the outer annulus through the gap at the junction of the cylinder and the cone. This effect is shown to be present in the single-particle trajectories in Figure 13. Both these effects have a tendency to reduce the collection efficiency of the coarse particles, thereby increasing the cut size, which is reflected in the data.

Another interesting feature of these grade efficiency curves is that as the speed of the fan increases, the sharpness of separation (roughly indicated by the slope of the curve around d_{50}) decreases. This can be explained as follows. In the case of angular vanes, the main forces, that is, the drag force and the centrifugal force, will be acting in opposite directions at the gap between the conical and the cylindrical section of the classifier. The primary roughing classification is generated by the combination of the centrifugal and drag forces at the feed plate level. Very fine particles are carried away by the secondary current, whereas large particles are thrown off this secondary stream and fall down into the conical section. When they reach the gap, the higher centrifugal force enables some of the lighter particles to escape into the annulus section because of the higher centrifugal force (arising from high tangential velocity in this region) and rebounding from the wall. Heavy particles, because of their large inertia, fall through this gap without being affected by this. Thus, this gap acts as a second, finishing stage of the classification. Moreover, when the speed of rotation increases, the lighter particles are carried away into the outer annulus by the air. However, because of higher velocities even larger particles are also carried into the annulus section through the gap. This reduces the collection efficiency of the large particles, the result of which is decreased sharpness of separation. This effect can be seen in Figure 14b, where the collection efficiency of the small-size particles is relatively unaffected by increase in speed, whereas that of the larger size particles is reduced.

Effect of Feed Rate. The measured effect of feed rate on the cut size (d_{50}) is opposite to that of increasing speed: increasing feed rate decreases the cut size. This can be attributed to the momentum coupling between the dispersed phase (that is, the particles) and the continuous phase (that is, the circulating air). The air loses momentum in accelerating the particles from their initially small velocity to nearly the tip speed. Note that most of the change in the particle velocity occurs after it is released from the feed plate. This momentum loss is proportional to the particulate flow rate. Also, the higher this momentum loss, the less strong will be the secondary circulation. As the secondary circulation diminishes, its ability to carry away particles also decreases, resulting in increased collection efficiencies for particles in the borderline, that is, those that are just able to be carried away by the air stream. This shifts the grade efficiency curves to the right, resulting in an increased d_{50} as the feed rate is increased. This situation is reflected well in the typical variation of the grade efficiency curves shown in Figure 14b.

Effect of Type of Vanes. It is shown above that the type of stationary guide vanes—radial or angular—makes a substantial difference to the flow pattern within the classifier. Specifically, it changes the orientation of the secondary circulation pattern in the cylindrical part of the classifier. The effect of this on the classification process has been found to be profound and is summarized in Figure 15. In Figure 15a, the relative coarse split, defined as the ratio of the mass of feed collected in the coarse stream to the total mass collected in the coarse and fine streams, is plotted as a function of the fan speed with rice husk as the feed material. The relative coarse split varies between 0 and 1 and for good classification, it should be close to 0.5, indicating that the feed stream containing a range of particle sizes is split into significant (measurable) amounts of coarse and fine fractions. If the value is close to zero, then it means nearly all the material is collected in the fines, and if the value is close to unity, then nearly all the material is collected in the coarse stream. Neither extreme would indicate satisfactory operation of the classifier.

With this interpretation of the relative coarse split, it can be seen from Figure 15a that the range of operability of the classifier is vastly different for the radial and the angular vane configurations. For the radial vane configuration, typical operating speeds are in the range of 500 to 1000 rpm, whereas for the angular vane configuration, they are in the range of 1500 to 2400 rpm. If the classifier is operated beyond these ranges, then poor classification would result with the feed being collected almost entirely in one of the two product streams. Typical

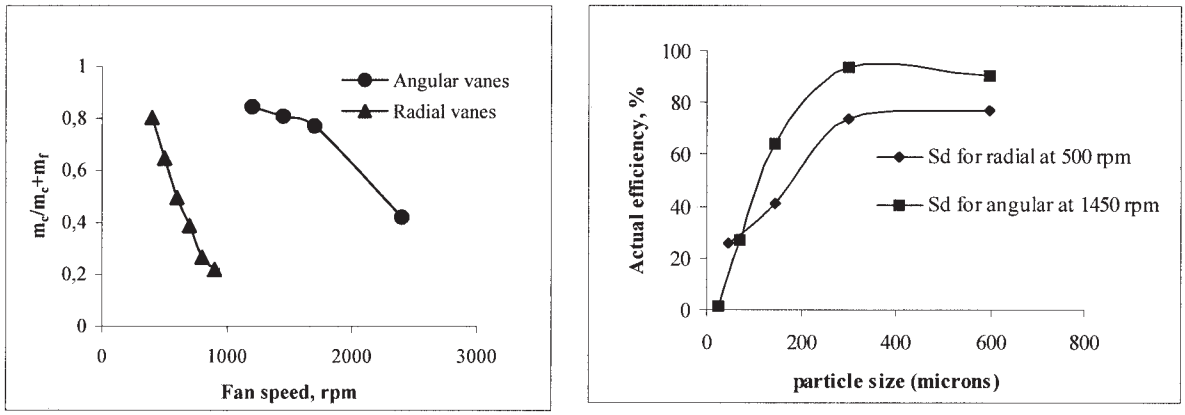

Figure 15. Variation of operating conditions with angular and radial stationary vanes.

(a) Relative coarse split; (b) grade efficiency curve for rice husk at a feed rate of 40 kg/h.

grade efficiency curves obtained with the two configurations are shown in Figure 15b for the case of rice husk at a feed rate of 40 kg/h. Note that, although the grade efficiency curves are similar, the rotational speeds in the two cases are very different: 500 rpm for the radial vanes and 1450 rpm for the angular vanes. Although the speed of rotation for angular vanes is higher (requiring more power for operation) for similar efficiency, there is less mass split at the coarse and fine ends, less cut size, and more sharpness of separation for the angular vanes.

The above results show that the operating characteristics for angular and radial vanes are quite different. These differences can be attributed to the flow pattern and the particle behavior within the classifier in the following way. One of the principal reasons for the lower speeds of operation for the radial vane configuration is the orientation of the secondary circulation, which is such that, at the gap between the conical and the cylindrical sections, both the air drag and the centrifugal force act in the radially outward direction. This helps in pushing the particle into the outer annulus to be eventually collected in the fine stream. Because both these forces increase with increasing speed, nearly all the feed material is pushed into the outer annulus, resulting in very low values of the relative coarse split. At the other extreme of low speeds, there is very little circulation of air induced and the centrifugal force is also very low to push the particles into the outer annulus. This leads to very high values of the relative coarse split. With the angular vanes, higher speeds are required to increase the centrifugal force to such an extent that it can overcome the air drag and push the large particles into the outer annulus, as explained earlier. Thus, the operating speed for an angular vane configuration is higher.

The higher mass splits at either end and the lower sharpness of separation for the radial vane configuration, compared to the angular vane configuration, can also be attributed to the flow pattern and the consequent alignment of the forces acting on the particles. Very fine particles will be entrained by the secondary circulation and, as they go through the radial vanes, they are more likely to be thrown into the inner cylindrical section than into the outer annulus by the radially inward centrifugal forces at the cone–cylinder junction. Once they are in the inner section, they may be collected in the coarse fraction by turbulent dispersion. This results in high mass split at the low (fines) end. Very large particles suffer higher centrifugal force and may therefore be pushed into the outer annulus, resulting in high mass split at the high (coarse) end. These higher mass splits at either end coupled with reduced collection efficiency for larger particles (arising from higher centrifugal force) also reduce the sharpness of separation in the radial vane configuration.

Conclusions

The flow field inside a rotating wheel air classifier has been calculated using CFD techniques, taking full account of the internal geometrical features. The predicted overall flow rate and the flow pattern are in good agreement with measurements and flow visualization studies. The calculations show that the induced flow depends strongly on geometric parameters such as the location of the inlet and outlet ports and the type of shutters used. Although the overall flow is circumferential, a strong internal recirculating flow is created within the upper part of the classifier, the direction of which is crucially dependent on the shutter type. The volumetric flow rate involved in this recirculation is about twice the net volumetric flow rate through the classifier.

Trajectory calculations of single particles show that the particle motion is influenced principally by centrifugal force, air drag, and wall-rebound characteristics. Particles of intermediate size (between 50 and 200 μm) for the conditions under study are influenced primarily by air drag, whereas large particles are influenced significantly by wall rebound. The wall rebound is possibly one of the means of how large particles enter the fines stream.

Experiments of the classification using angular and radial shutter vanes show distinct range of operability of each type. These results can be interpreted coherently in the light of the flow pattern and particle trajectory calculations. Thus, these results illustrate the strong coupling between the flow pattern and the classification characteristics. Appreciation of this linkage helps in interpreting better size classification results. Detailed measurements of the velocity, turbulence, and particle fields will help validate the present results in addition to throwing further light on the working of the classifier.

Acknowledgments

Calculations reported here have been carried out using the computational facilities of the CFD Centre, IIT-Madras, India.

Literature Cited

American Institute of Chemical Engineers (AIChE), *AIChE Equipment Testing Procedure. Particle Size Classifiers*, 2nd ed. AIChE, New York, pp. 1–64 (1993).

Bakker, A., A. H. Haidari, and L. M. Oshinowo, "Realize Greater Benefits from CFD, CEP," *AIChE J.*, **47**, 45 (2001).

Clerc, L., M. Minoux, and A. Benhassaine, "Pneumatic Selection of Flyash: Selection Methods—Influence of the Operating Parameters," *Powder Technol.*, **105**, 172 (1999).

Ferziger, J. H., and M. Peric, *Computational Methods for Fluid Dynamics*, Springer-Verlag, Berlin, Germany (1996).

Galk, J., W. Peukert, and J. Krahnen, "Industrial Classification in a New Impeller Wheel Classifier," *Powder Technol.*, **105**, 186 (1999).

Griffiths, W., and F. Boysan, "Computational Fluid Dynamics (CFD) and Empirical Modelling of the Performance of a Number of Cyclone Separators," *J. Aerosol Sci.*, **27**(2), 281 (1996).

Haider, A., and O. Levenspiel, "Drag Coefficient and Terminal Velocity of Spherical and Non-Spherical Particles," *Powder Technol.*, **86**, 63 (1989).

Kolacz, J., "Investigating Flow Conditions in Dynamic Air Classification," *Miner. Eng.*, **15**, 131 (2002).

Launder, B. E., and D. B. Spalding, *Lectures in Mathematical Models of Turbulence*, Academic Press, London (1972).

Lynch, A. J., *Mineral Processing and Grinding Circuits, Their Simulation, Optimization, Design and Control*, Elsevier Scientific, Amsterdam (1977).

Murthy, J. Y., S. R. Mathur, and D. Choudhury, "CFD Simulation of Flows in Stirred Tank Reactors Using a Sliding Mesh Technique," *IChemE Symp. Ser.*, 136, 341 (1994).

Patankar, S. V., *Numerical Heat Transfer and Fluid Flow*, Hemisphere, Washington, DC (1980).

Shekhar, S. M., and S. Jayanti, "Mixing of Pseudoplastic Fluids Using Helical Ribbon Impellers," *AIChE J.*, **49**, 2768 (2003).

Snow, R. H., H. K. Brian, C. Edward, and C. Guggilam, *Perry's Chemical Engineers Handbook*, 6th ed., Sect. 8, McGraw-Hill, New York (1984).

Wang, Q., M. C. Melaaen, and S. R. De Silva, "Investigation and Simulation of a Cross-Flow Air Classifier," *Powder Technol.*, **22**, 273 (2001).

Wilcox, D. C., *Turbulence Modelling for CFD*, Griffin Printing, Glendale, UK (1993).

Wills, B. A., *Mineral Processing Technology*, 5th ed., Camborne School of Mines, Cornwall, UK (1992).

Manuscript received July 6, 2004.